Dynamics of Octadecylphosphonate Monolayers Self-Assembled on Zirconium Oxide: A Deuterium NMR Study

C. T. Yim*

Department of Chemistry, Dawson College, 3040 Sherbrooke Street West, Westmount, Québec, Canada H3Z 1A4

S. Pawsey, F. G. Morin, and L. Reven

Department of Chemistry, McGill University, 801 Sherbrooke Street West, Montréal, Québec, Canada H3A 2K6

Received: September 28, 2001; In Final Form: December 3, 2001

Deuterium NMR spectroscopy has been used to probe the dynamics of deuterated octadecylphosphonate (−1,1−d_2) (ODPA−d_2) monolayers on nonporous ZrO_2 powder (surface area ≈ 40 m^2/g) over the temperature range of 200−340 K. At 200 K, a broadened Pake doublet with distinct nonrigid characteristics and a horn splitting of approximately 120 kHz was observed. With increasing temperature, the ^2H spectrum gradually transforms into a relatively narrow and featureless peak. Spectral simulations are performed with the help of plausible motional models, and the results show that, over the whole temperature range studied, the C_1−D bonds have substantial motional freedom with respect to the characteristic ^2H NMR time scale. In addition, at each temperature, a weighted superposition of several simulated line shapes with different rates and site populations is required to account for the observed spectral features, indicating the presence of considerable motional heterogeneity within the ODPA monolayers. The results are further discussed in terms of the known characteristics of the ZrO_2 surface and of the conformational transitions in the octadecyl chain.

Introduction

It has been known since the 1960s that phosphonic acids react with a wide range of alkali and transition metals to form lamellar metal phosphonates.[1] Recently, self-assembled monolayers and multilayers based on these metal phosphonates have generated considerable interest because of their potential for controlling the surface molecular architecture and their relative ease of preparation. Alkyl phosphonates can be adsorbed as strongly bound monolayer films on a variety of different metal oxide surfaces.[2] Metal phosphonate multilayers can be prepared by alternately dipping an appropriately functionalized substrate into solutions of metal ions and bisphosphonic acids.[3] The abilities of these self-assembled systems to modify surface properties have been exploited for a number of different applications including nonlinear optical materials,[4,5] chemical sensing,[6] and solar energy storage devices.[4,7]

Over the past few years, we have employed solid-state NMR techniques for structural and dynamic characterization of a number of self-assembled monolayers (SAMs).[8] In regard to metal phosphonate SAMs, these studies reveal that alkylphosphonic acids bind strongly to nonporous ZrO_2 powder primarily via a monodentate surface bond.[2] The broad peak in the ^{31}P CPMAS spectrum also reveals the presence of considerable bonding heterogeneity in the monolayer. The ^{13}C NMR data suggest that at room temperature, the alkyl chains in the OPDA−ZrO_2 monolayer have transoid segments albeit with a significant amount of gauche defects, and the number of chains in less ordered conformations increases upon heating reflecting a gradual thermal disordering of the octadecyl chains.[9] The two-dimensional ^{31}P NMR exchange spectrum of the same system taken at room temperature indicates the phosphonate headgroups are static during the 10 ms mixing time, although with a longer mixing time of 500 ms reorientation of the headgroups becomes detectable.[10] To further probe the dynamics of the octadecyl chain, we have conducted a detailed ^2H NMR study. Among the commonly accessible nuclei in NMR, the deuteron has been a particularly popular probe for the study of molecular dynamics and organization in solids and in other anisotropic systems, such as lipid bilayers,[11] polymers,[12] liquid crystals,[13,14] and interfacial regions.[15] Interesting ^2H NMR studies have been conducted on the dynamics of alkyl chains in alkylsilyl-modified silica gel and in alkanethiolate monolayers.[16,17] Deuterium line shapes and spin relaxation behaviors have also been determined for several surface-bound surfactant molecules.[18−20] Deuterium NMR is dominated by quadrupolar interactions and is almost exclusively governed by the motions and orientation of the deuteron-containing bond (e.g., the C−D bond) relative to the applied magnetic field. The reorientation motions of the C−D bonds modulate the quadrupolar interactions and thus affect the observed line shape and spin−lattice relaxation time. Motions having rates comparable to the observed line width, i.e., 250 kHz, strongly affect the intensity and shape of the signal. In most cases, detailed line shape analyses lead to valuable information regarding the type, the amplitude, and the rate of the motion involved. Various motional models have been proposed, and the evaluation of the amplitudes and rates of these motions from the observed spectra is usually accomplished with the help of line shape simulations.[21,22]

* To whom correspondence should be addressed. Tel.: (514) 931-8731. Fax: (514) 931-3567. E-mail: c.yim@mcgill.ca.

10.1021/jp013649e CCC: $22.00
Published on Web 01/16/2002

In this paper, we report the measurements of ^{2}H NMR spectra of deuterated octadecylphosphonate ($-1,1-d_2$) (ODPA$-d_2$) adsorbed on nonporous ZrO_2 powder. The spectra were acquired as functions of temperature and of echo delay time τ. The dynamics of the bound ODPA$-d_2$ molecules are discussed, and the data are further analyzed to yield plausible models for the motions involved.

Experimental Section

Synthesis of ODPA$-1,1-d_2$. Stearic acid (from Anachemia Chemical Ltd., Montreal, Canada) was converted to 1,1$-d_2-$octadecanol by reduction with $LiAlD_4$ (from Aldrich, 98 atom % D).[17] Bromination of 1,1$-d_2-$octadecanol followed by the Michaelis$-$Arbuzov reaction of 1,1$-d_2-$octadecyl bromide with triethyl phosphite yielded 1,1$-d_2-$octadecylphosphonic acid[23] after hydrolysis. The crude product was further purified by recrystallization with acetone.

Monolayer Preparation. Nonporous zirconia (ZrO_2) powder, from Degussa (surface area $\approx$ 40 m^2/g, diameter $\approx$ 30 nm) was calcinated at 400 °C for at least 8 h to eliminate any residual organic impurities before use. Three times the amount of ODPA$-d_2$ needed to form a monolayer was dissolved in methanol, while ZrO_2 powder was dispersed in Millipore water by sonication. The dispersed ZrO_2 powder was mixed in with the acid solution, and the total volume was brought up to 700 mL. The resulting mixture with a methanol/water ratio of 3:1 was left to reflux for 2 days, followed by an additional 2 days of annealing. The powder was then filtered off and washed with copious quantities of methanol five times to remove any unbound surfactant. Elemental analyses show that the carbon content of the monolayer sample is 4.56%. Assuming a surface area of 40 m^2/g for the ZrO_2 powder and 24×10^{-20} m^2 area/ODPA molecule, the surface coverage was estimated to be 82%.

NMR Measurements. The sample for ^{2}H NMR measurements was prepared by tightly packing ~600 mg of ODPA$-d_2/ZrO_2$ powder into a shortened 10-mm NMR tube. The ^{2}H NMR spectra were acquired with a Chemagnetics CMX-300 spectrometer operating at 45.99 MHz using the phase cycling quadrupolar echo sequence ($(\pi/2)_x - \tau - (\pi/2)_y - \tau -$ acquisition - - - -). The acquisition conditions and parameters were as follows: number of acquisitions, 7000$-$8000; $\pi/2$ pulse length, 4.0 μs; acquisition recycle time, 1.0 s; dwell time, 1.0 μs; pulse delay time τ, 20$-$80 μs. After Fourier transformation, the resulting spectra were further symmetrized by reversing the recorded pattern through the zero frequency line and adding to itself. The signal intensity was measured from the height of the echo maximum.

Simulations of deuterium powder line shapes were performed with a modified Wittebort program.[21,24] All calculated line shapes were corrected for finite pulse length and convoluted with a Lorentzian broadening of 1.5 kHz.

Results and Discussion

Figure 1 shows the quadrupole echo spectra of the monolayer sample, recorded with $\tau = 20$ μs, as a function of temperature. At 200 K, a broadened Pake doublet with a horn splitting of 120 kHz was observed. With increasing temperature, the relative intensity of the central portion of the spectrum gradually increases with respect to that of the two horns, and at 343 K, a relatively narrow and featureless peak is observed. However, up to room temperature, the breadth of the powder spectra remains more or less unchanged at approximately 120 kHz, suggesting that one of the transverse principal components of the field gradient tensor is not significantly affected by the underlying motional process.

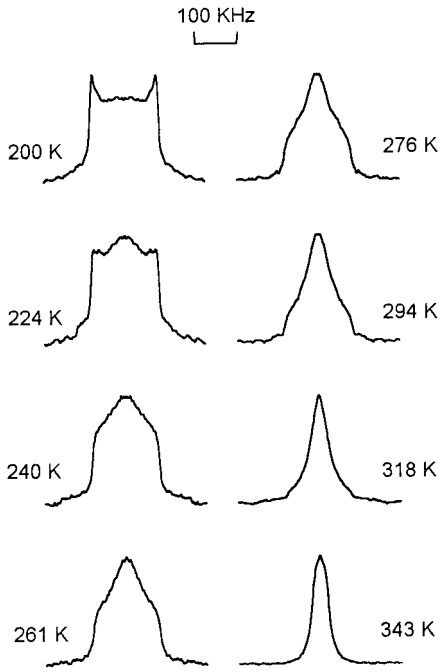

Figure 1. ^{2}H NMR spectra of ODPA$-d_2$ adsorbed on ZrO_2 at various temperatures, recorded with pulse spacing $\tau = 20$ μs.

In Figures 2 and 3, the ^{2}H spectra of ODPA monolayers, at several selected temperatures (200, 240, 276, and 318 K), are shown as a function of pulse delay time τ in the quadrupolar echo sequence. The number adjacent to each line shape is the echo intensity (i.e., the signal intensity) normalized to the intensity of $\tau = 20$ μs. These spectra demonstrate that at each temperature there are significant variations in both the line shape and signal intensity with delay time τ.

The structures and thermal properties of self-assembled monolayers formed by functionalized long-chain hydrocarbons have been shown to resemble those of lipid analogues.[8] In the studies of the gel phases of lipid bilayers, several simple and physically meaningful motional models have been employed to simulate the observed ^{2}H NMR spectra.[11b,25] These models will be considered for simulating our experimental ^{2}H spectra. Since the monolayer systems studied here are highly heterogeneous,[26] motions with complicated trajectories and with distributions in both the rate and amplitude are expected. Therefore, our aim is not to achieve an exact fit to the observed data but to evaluate simple models so as to determine whether they can account for the important spectral features and trends. By adopting this approach, we expect to reveal the essential attributes of the dynamic processes involving alkyl chains.

First, we consider the restricted two-site trans$-$gauche isomerization model (referred to as the two-site model in further discussions). The model describes the reorientation of the C$-$D bond vectors between two sites that are related by a jump angle of approximately 110°. Because of the inter- and intramolecular interactions, one of the sites is more populated and will be referred to as the trans site. As pointed out by Hirschinger and English,[27] two-site jumps are planar motions, and therefore, one of the transverse principal components of the field gradient tensor (FGT) is not affected by the motion. This constant principal component of FGT would in turn lead to powder spectra with a constant breadth of 120 kHz. The fact that our experimental spectra do show a more or less constant breadth of this magnitude over the temperature range of 200$-$290 K

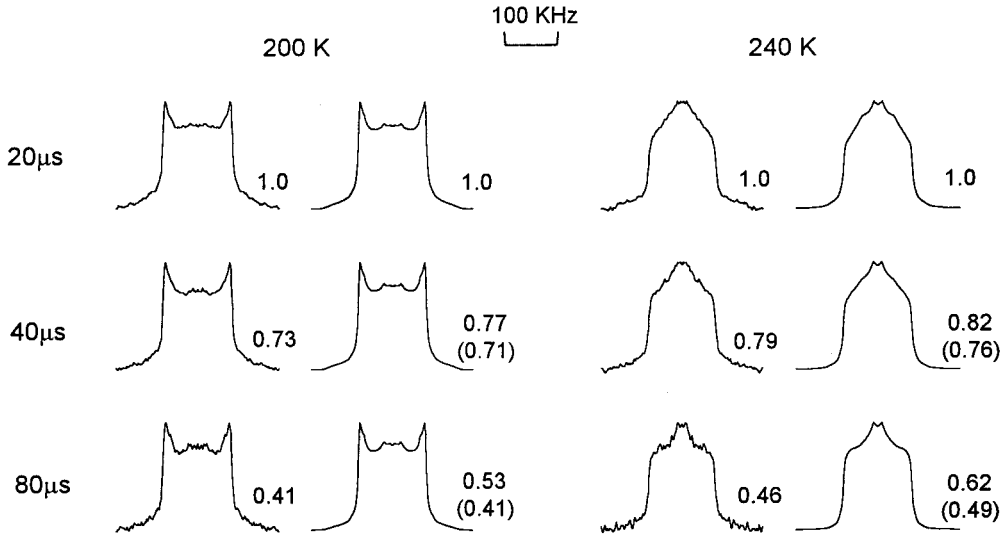

Figure 2. Experimental (left) and simulated (right) ^{2}H NMR spectra of ODPA−1,1−d_2 on ZrO_2, at 200 and 240 K with $\tau = 20$, 40, and 80 μs. The number adjacent to each line shape is the corresponding echo intensity normalized to the $\tau = 20$ μs intensity.

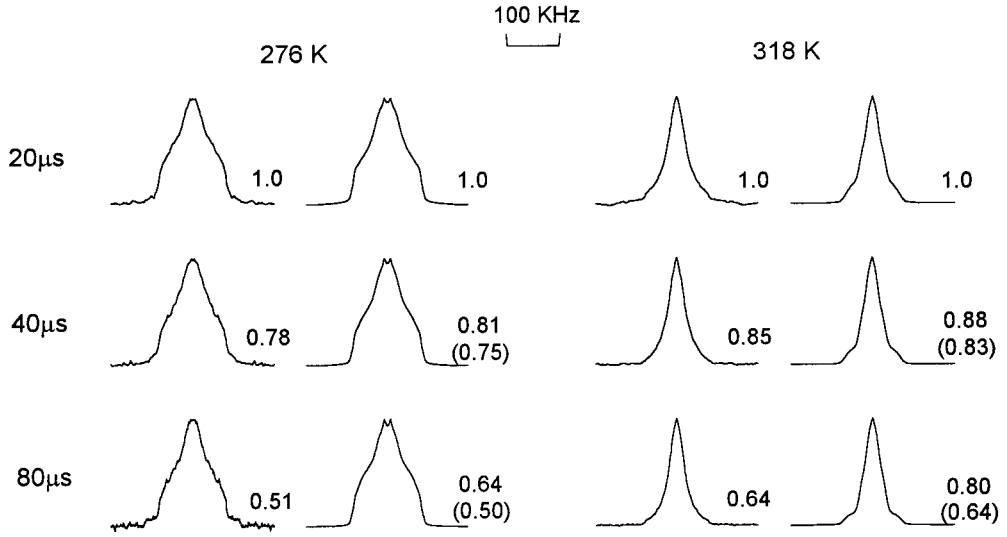

Figure 3. Experimental (left) and simulated (right) ^{2}H NMR spectra of ODPA-1,1−d_2 on ZrO_2, at 276 and 318 K with $\tau = 20$, 40, and 80 μs. The number adjacent to each line shape is the corresponding echo intensity normalized to the $\tau = 20$ μs intensity.

suggests the use of the two-site model for simulations. More detailed line shape analyses show that, with superpositions of several simulated line shapes having different rates and site populations, this model indeed leads to reproduction of the experimental spectra and their variations with echo delay time τ for the two lowest temperatures studied. However, for temperatures equal to and higher than 240 K, it failed to generate line shapes in reasonable agreement with the experimental spectra. In particular, superpositions of simulated line shapes calculated from this model will not yield the triangular top, a common feature present in all these spectra.

To remedy the situation, we turn to the six-site jumping model, originally devised for analyzing ^{2}H spectra of alkyl chains undergoing axial diffusion.[25] This model and its variations have since been employed in studies of other systems.[16,28] To model the axial diffusion, the chains are allowed to execute 3-fold (120°) rotational jumps around their long axis. In a tetrahedral lattice, there are only two possible angles between C−D vectors and the all-trans chain axis: 90° and 35.3°, corresponding to trans and gauche sites, respectively. Thus, the 3-fold jumping scheme leads to a six-site model: three trans sites with C−D bonds lying in a plane perpendicular to chain axis and three gauche sites on a cone at an angle of 35.3° with respect to the chain axis. The sites can have different populations, P_t and P_g, reflecting the ratio of trans and gauche conformers. In addition to rotational jumps, also allowed are trans-gauche transitions involving exchanges of C−D bonds in the perpendicular plane and on the cone. Thus the model calls for two different types of jumping rates: the 3-fold rotational jump rate (Ω_{rot}) for simulating axial diffusions, and the isomerization rates, $\Omega_{t\rightarrow g}$ and $\Omega_{g\rightarrow t}$. Figure 4 shows the orientations of the trans and gauche sites and the kinetic scheme for the spectral simulation.

If isomerization ($\Omega_{t\rightarrow g} \rightarrow 0$ or $P_g \rightarrow 0$) is negligible and the 3-fold jumping rate is fast on the ^{2}H NMR time scale ($\Omega_{rot} > 10^7$), one would observe a Pake pattern with its breadth reduced to half of its static value, i.e., with the horn separation $\approx$ 62 kHz. We notice that none of the experimental spectra in Figure 1 show anything resembling a reduced Pake pattern. Furthermore, as described in the Introduction, the two−dimensional ^{31}P NMR data indicate that, at room temperatures, the headgroup remains rigid on the deuterium NMR time scale. It is also hard to envisage axial diffusion of the tethered chains without the participation of the headgroup or without severely disrupting

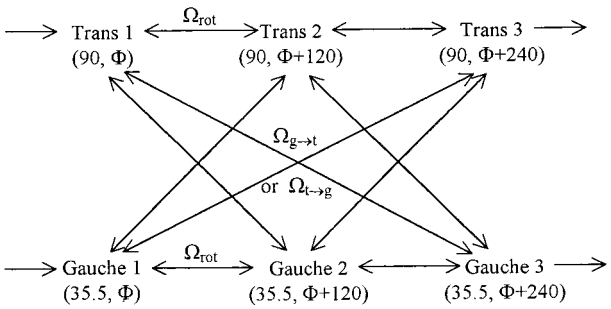

Figure 4. Kinetic scheme for the six-site jump model. Orientation of the sites is specified by the polar coordinates (ϑ,Φ) with respect to the all-trans chain axis (see text). Double arrow indicates the allowed transitions. Ω_{rot} is the jump rate between two trans or two gauche sites; $\Omega_{g\rightarrow t}$ and $\Omega_{t\rightarrow g}$ represent trans−gauche isomerization rates.

the chain packing in the monolayers. On the basis of these arguments, it seems appropriate to assume the absence of axial diffusion around the long axis of the alkyl chain in our phosphonate monolayers and to set Ω_{rot}, the 3-fold rotational jumping rate, to zero.

With $\Omega_{rot} = 0$, the six-site model represents a less restricted isomerization scheme due to the higher number of sites accessible to reorientational motions. Since the motion is no longer planar, all three principal components of FGT are affected, and the resulting width of the powder spectra could be much less than 120 kHz. In fast motion limits, the model predicts a Pake pattern with horn splitting $\Delta\nu$ given by

$$\Delta\nu = (1/2)(1-2P_g)\Delta\nu_{static} \qquad (1)$$

With $P_t = P_g = 0.5$, $\Delta\nu = 0$ and the broad powder pattern reduces to a line.

In summary, the motional models assumed for spectral simulations are (a) the two-site model with a jump angle set at 111° and (b) the six-site model with $\Omega_{rot} = 0$. In all simulations, a quadrupole coupling constant of $Q_{CC} = 168$ kHz and an asymmetry parameter of $\eta = 0$ are assumed. With either model, the motions are characterized by jump rates $\Omega_{t\rightarrow g}$ and $\Omega_{g\rightarrow t}$ and site populations P_t and P_g. In addition to $P_t + P_g = 1$, these parameters must satisfy microscopic reversibility: $P_t\Omega_{t\rightarrow g} = P_g\Omega_{g\rightarrow t}$, and therefore, only two of the four parameters are independent.

At almost all the temperatures studied, it was found that reasonable fits with the experimental spectra could only be achieved by a weighted superposition of three of four line shapes[29] computed assuming different rates and site populations. In addition, it has also been found that a better agreement can be achieved if we assumed a distribution in P_g values for the six-site model as first suggested by Zeigler and Maciel:[16]

$$f(P_g) = C\{\exp[-(P_g - P_g(\max))^2/2\sigma^2]\} \qquad (2)$$

where C is the normalizing constant and P_g (max) and σ define the maximum and width of the distribution. In all our simulations, the width σ is fixed at 0.05, except at the highest temperature (343 K) for which a value of 0.10 is assumed. Since σ remains constant, adopting P_g distribution does not introduce additional parameters.

For the two lowest and two highest temperatures, component line shapes are computed with the two-site and six-site models, respectively. At intermediate temperatures line shapes originating from both motional models contribute to the simulated spectra. Examples of these simulated line shapes and their relative intensities (the number adjacent to the corresponding line shape) are also presented in Figures 2 and 3. Although the simulated line shapes are in reasonable agreement with the experimental spectra, all simulated signal intensity show a weaker τ dependence.

It should be pointed out that the spectral simulations did not include the additional intensity decay arising from $^1H-^2H$ dipolar couplings. The echo intensity decay due to dipolar interactions is usually assumed to be an exponential function of pulse delay τ with a time constant T_{2d}.[30,31] Since relevant data are not available for this system, a rough estimate are obtained from results for other systems; T_{2d} values of 200−300 μs have been used to simulate the ^2H NMR spectra of oligonucleotides, polymeric and surface bound systems.[20,30,31] It has also been found that these values remain more or less constant with changes in temperature. Thus, a T_{2d} value of 250 μs was chosen to calculate the additional echo intensity decay for our system. The calculated intensities, normalized to the $\tau = 20$ μs intensity and presented in brackets in Figures 2 and 3, indeed show better agreement with the experimental values.

The parameters used for simulating the spectra, including those shown in Figures 2 and 3, are summarized in Table 1. The estimated relative errors for these parameters depend on their magnitude; roughly speaking, they are ±20% for gauche populations and for component weights and ±(0.4 decade) for the reported rates (i.e., $\log((\Omega_{reported} + \Delta\Omega)/\Omega_{reported}) = \pm 0.4$).

Each component line shape in Table 1 and its associated motion are characterized by four parameters: the jump rate Ω, the site population P_g, the jump angle, and the number of sites accessible to the motion. These parameters describe different characters of molecular motions. We also notice that the last two parameters are fixed with the choice of model and the jump angles are very similar for the two models. For motions belonging to the same model, the product of the rate and its corresponding population such as $P_t\Omega_{t\rightarrow g}$ or $P_g\Omega_{g\rightarrow t}$ ($= P_t\Omega_{t\rightarrow g}$) has been used as a quantitative measure of molecular mobility.[28b] Comparison of these motions can thus be made by quoting the ($P\Omega$) values which are listed in the last column of Table 1. Unfortunately, similar quantities or criteria are not available for comparing motions described by two different motional models.

In simulation of spectra, we have superimposed line shapes calculated with different models, as well as those calculated with different rates and site populations. As expected, the number of components from the less restricted six-site model increases with increasing temperature. Due to the lack of criteria for comparing parameters of different motional models, we are unable to identify which of the two-site components is being replaced by the new six-site components with the increase in temperatures and to provide rationales for the relative magnitudes of their parameters such as rates and site populations. At extreme temperatures where most or all rates become either very fast or very slow in comparison with the deuterium NMR time scale, the difference in rates has a diminishing effect on the observed line shape. Therefore, the number of component line shapes required to reproduce the experimental spectra decreases at both the low- and high-temperature sides.

The simulation results show that, over the whole temperature range studied, the C_1-D bonds in ODPA monolayers have substantial motional freedom. However, another monolayer system, i.e., octadecanethiol monolayers on gold ($C_{18}S/Au$), show quite different behavior;[17] the ^2H NMR spectra of 1,1−d_2−$C_{18}S/Au$ indicate that, at or below room temperature, C_1-D bonds remain essentially static on the characteristic ^2H NMR time scale. Several plausible explanations could be advanced for the observed difference. For example, the substantial

TABLE 1: Spectral Simulation Parameters for the ODPA-ZrO_2 System

temp (K)	motional model	rate $\Omega_{t\rightarrow g}$ (s^{-1})	gauche population P_g	component weight	mobility $P\Omega$	temp (K)	motional model	rate $\Omega_{t\rightarrow g}$ (s^{-1})	gauche population P_g	component weight	mobility $P\Omega$
200	2-site	1.6×10^3	0.188	0.80	2.98×10^2	276	2-site	9.5×10^6	0.413	0.32	3.94×10^6
	2-site	3.2×10^5	0.063	0.10	1.99×10^4		6-site	1.4×10^3	0.175	0.34	2.51×10^2
	2-site	3.2×10^6	0.313	0.10	9.95×10^5		6-site	4.8×10^5	0.025	0.28	1.19×10^4
							6-site	9.5×10^6	0.200	0.06	1.91×10^6
224	2-site	1.3×10^3	0.200	0.44	2.55×10^2	294	2-site	1.3×107	0.450	0.30	5.73×10^6
	2-site	1.4×10^5	0.113	0.26	1.61×10^4		6-site	9.5×10^4	0.150	0.18	1.43×10^4
	2-site	5.6×10^5	0.350	0.26	1.95×10^5		6-site	9.5×10^5	0.050	0.42	4.77×10^4
	2-site	1.6×10^7	0.413	0.04	6.57×10^6		6-site	9.5×10^6	0.300	0.10	2.86×10^6
240	2-site	2.4×10^5	0.213	0.46	5.07×10^4	318	6-site	1.1×10^5	0.100	0.62	1.11×10^4
	2-site	2.0×10^5	0.475	0.08	9.45×10^4		6-site	1.6×10^7	0.350	0.19	5.57×10^6
	2-site	1.6×10^6	0.388	0.24	6.17×10^5		6-site	4.0×10^7	0.150	0.19	5.97×10^6
	6-site	1.3×10^3	0.050	0.22	6.37×10^1						
261	2-site	9.5×10^6	0.350	0.22	3.34×10^6	343	6-site	4.0×10^7	0.270	1.00	1.08×10^7
	2-site	9.5×10^6	0.475	0.16	4.54×10^6						
	6-site	1.6×10^3	0.075	0.40	1.19×10^2						
	6-site	2.0×10^5	0.150	0.22	2.98×10^4						

motional freedom for ODPA can be attributed to the large size of the phosphonate headgroup allowing more free volume available to reorientation motions. The cross section of the phosphonate headgroup is ~24 Å^2, which is large when compared with 18 Å^2 for the cross section of alkyl chains in crystalline polyethylene. As concluded in our earlier work, the primary mode of attachment of ODPA on ZrO_2 surface is monodentate rather than tridentate, and as a consequence, the three phosphonate oxygen bonds are definitely not equivalent, and the phosphonate alkyl chains are probably oriented perpendicular to the substrate surface.[9,32] By comparison, the area occupied by the octadecanethiolate chain in $C_{18}S$/Au is 21.7 Å^2, and the chains have large tilt angles of 30° with respect to the surface normal. The nearly perpendicular orientation adopted by the alkyl chain in ODPA would provide more free space and lessen van der Waals interactions between the chains.[33]

The number of line shapes utilized in simulations suggests the presence of at least four types of octadecyl chains in the monolayers with very different mobilities, as illustrated by the large differences in their kinetic parameters (rates, gauche populations, and numbers of accessible sites). Furthermore, the component weights show considerable variations with temperature, suggesting the absence of well-defined domains with respect to the orientational freedom of the alkyl chain. We interpret the varying weights as an indication that there are two or more factors affecting the reorientational freedom. The surface of zirconium oxide is known to contain many different types of surface sites,[26] and as a consequence, the surface-bound phosphonates experience a range of different environments, as evidenced by the broad isotropic peak observed in the ^{31}P NMR spectra. Recently, the possibility of intermolecular hydrogen bonding between the adsorbed species has also been suggested.[34] Motional freedoms are also expected to be affected by other factors such as packing densities and chain tilt angles. Therefore, we consider the observed motional heterogeneity as a reflection of both the heterogeneous bonding environment on the ZrO_2 surface and the variations in other additional factors.

It is of interest to note that the high mobility does not reflect a low conformational order for the alkyl chain as revealed by the ^{13}C NMR data. The line shape simulation yields jump rates between different sites, each characterized by the C−D bond orientation and its relative population. The motional models do not specify how the motions actually occur. For example, it has been argued that the trans-gauche isomerization in closed packed alkyl chain mostly involves cooperative motions such as 3-bond motions leading to the formation of kinks. The so-called kink migration involves simultaneous conformation transitions at several positions along the alkyl chain while the number of gauche defects in the chain remains unchanged. In addition, with tethered alkyl chain systems, a conformation transition occurring at an "upstream" C−C bond changes the orientations of the "downstream" C−D bonds even though the conformations of the downstream C−C bonds remain unchanged. Thus, the transitions between sites with different C−D orientations can proceed via several different routes. While conformational transitions do lead to changes in orientations, the sites in motional models cannot be simply identified as trans and gauche sites of a particular C−C bond. Without detailed knowledge of the motional processes, a unique relationship cannot be established between the site populations in motional models and the gauche defects in the alkyl chain. Therefore, it is not possible to infer the conformational state of the whole chain on the basis of the simulated site populations concerning the orientations of C_1−D bond. In this respect, we notice the interesting molecular dynamics simulation results of Biswas and Schürmann on alkyl chains with fixed headgroups in model bilayers.[35] With the increase of free surface area per molecule, detailed simulation analyses show that additional gauche defects appear mainly at the chain extremities, i.e., at both the free end and in the region of the fixed headgroups. While the increase in gauche content at the free end is expected, the increase in defects near the headgroups can be traced back to the tendency of alkyl chains to optimize the interchain separations which lead to the formation of ordered clusters and thus more additional defects near the tethered ends. Molecular dynamics simulation of stiff polymers with flexible side chains has also been performed and yielded similar results; i.e., more gauche defects are present at both ends of the side chain than in the center.[36]

Conclusions

We have outlined two motional models that can account for the important spectral features and trends. The models have furnished a useful, although somewhat simplified picture which allows more quantitative discussion concerning the dynamics and the environment of the octadecylphosphonate molecules. Of course, this does not offer assurance that some other models will not fit the experimental data equally well or better and, at the same time, provide a more consistent picture. In particular, due to the lack of detailed information, our models do not explicitly address the effect of the headgroup and its bonding mode. We have also argued against the inclusion of axial

diffusion as a possible motional mode for our system, although by not involving conformational transitions, the axial diffusion model is capable of combining high mobility with a high degree of conformational order.[25b] However, we are of the opinion that the chosen models have yielded quantities that reflect the fundamental characteristics of the motions involved, specifically their amplitudes and their correlation times.

We have shown that, within the temperature range studied, the C_1-D bonds of the attached phosphonate molecules undergo reorientational motions with rates fast enough to affect the ^2H solid echo spectra. We attribute the fast reorientation rates to the large cross sectional area of the phosphonate headgroup and its monodentate binding mode on the ZrO_2 surface. While the motions at lower temperatures and their effect on the observed spectra can be satisfactorily described by the two-site model, the less restricted six-site model must be considered for spectral simulation at higher temperatures.

By spectral simulation, we have demonstrated that there exists substantial motional heterogeneity in phosphonate monolayers. The result primarily reflects the known heterogeneous bonding environment on the ZrO_2 surface as revealed by various experimental techniques.

Acknowledgment. Financial support in the form of operating grants from the Quebec Government (Fonds FCAR) is gratefully acknowledged.

References and Notes

(1) Cao, G.; Hong, H.-G.; Mallouk, T. E. *Acc. Chem. Res.* **1992**, *25*, 420.

(2) Gao, W.; Dickinson, L.; Grozinger, C.; Morin, F.; Reven, L. *Langmuir* **1996**, *12*, 6429.

(3) (a) Lee, H.; Kepley, L. J.; Hong, H.-G.; Mallouk, T. E. *J. Am. Chem. Soc.* **1988**, *110*, 618. (b) Lee, H.; Kepley, L. J.; Hong, H.-G.; Akhter, S.; Mallouk, T. E. *J. Phys. Chem.* **1988**, *92*, 2597.

(4) Katz, H. E. *Chem. Mater.* **1994**, *6*, 2227.

(5) Hanken, D. G.; Corn, R. M. *Anal. Chem.* **1995**, *67*, 3767.

(6) Mallouk, T. E.; Gavin, J. A. *Acc. Chem. Res.* **1998**, *31*, 209.

(7) Thompson, M. E. *Chem. Mater.* **1994**, *6*, 1168.

(8) (a) Badia, A.; Lennox, R. B.; Reven, L. *Acc. Chem. Res.* **2000**, *33*, 475. (b) Reven, L.; Dickinson, L. *Thin Films* **1998**, *24*, 149.

(9) Gao, W.; Dickinson, L.; Grozinger, C.; Morin, F.; Reven, L. *Langmuir* **1997**, *13*, 115.

(10) Dickinson, L. Ph.D. Thesis, McGill University, Montreal, Canada, 1998.

(11) (a) Seelig, J.; Macdonald, P. M. *Acc. Chem. Res.* **1987**, *20*, 221. (b) Griffin, R. G. *Methods Enzymol.* **1981**, *72*, 108. (c) Davis, J. H. *Biochim. Biophys. Acta* **1983**, *737*, 117.

(12) Spiess, H. W. *Adv. Polym. Sci.* **1985**, *66*, 23.

(13) Hoatson, G. L.; Vold, R. L. in NMR Basic Principles and Progress; Diehl, P.; Fluck, E.; Gùnther, R.; Kosfeld, R.; Seelig, J.; Eds; Springer-Verlag: Berlin, 1994; Vol. 32, p 1.

(14) Muller, K.; Meier, P.; Kothe, G. *Prog. Nucl. Magn. Reson. Spectrosc.* **1985**, *17*, 211.

(15) Grandjean, J. *Annu. Rep. NMR Spectrosc.* **1998**, *35*, 217.

(16) Zeigler, R. C.; Maciel, G. E. *J. Am. Chem. Soc.* **1991**, *113*, 6349.

(17) Badia, A.; Cuccia, L.; Demers, L.; Morin, F.; Lennox, R. B. *J. Am. Chem. Soc.* **1997**, *119*, 2682.

(18) Söderlind, E.; Stilbs, P. *Langmuir* **1993**, *9*, 2024; **1994**, *10*, 890.

(19) Macdonald, P. M.; Yue, Y.; Rydall, J. R. *Langmuir* **1992**, *8*, 164.

(20) Yim, C. T.; Brown, G. R.; Morin, F. *Langmuir* **1997**, *13*, 4383.

(21) Wittebort, R. J.; Olejniczak, E. T.; Griffin, R. G. *J. Chem. Phys.* **1987**, *86*, 5411.

(22) Greenfield. M. S.; Ronemus, A. D.; Vold, R. L.; Vold, R. R.; Ellis, P. D.; Raidy, T. R. *J. Magn. Reson.* **1987**, *72*, 89.

(23) Bhattacharya, A. K.; Thyagarajan, G. *Chem. Rev.* **1981**, *81*, 415.

(24) Yim, C. T.; Gilson, D. F. R.; Budgell, D. R.; Gray, D. G. *Liq. Cryst.* **1993**, *14*, 1445.

(25) (a) Huang, T. H.; Skarjune, R. P.; Wittebort, R. J.; Griffin, R. G.; Oldfield, E. *J. Am. Chem. Soc.* **1980**, *102*, 7377. (b) Blume, A.; Rice, D. M.; Wittebort, R. J.; Griffin, R. G. *Biochemistry* **1982**, *21*, 6220.

(26) (a) Schafer, W. A.; Carr, P. W.; Funkenbusch, E. F.; Parson, K. A. *J. Chromatogr.* **1991**, *587*, 137. (b) Nawrocki, J.; Dunlap, C. J.; Carr, P. W.; Blackwell, J. A. *Biotechnol. Prog.* **1994**, *10*, 561.

(27) Hirschinger, J.; English, A. D. *J. Magn. Reson.* **1989**, *85*, 542.

(28) (a) Ebelhauser, R.; Spiess, H. W. *Ber. Bunsen-Ges. Phy. Chem.* **1985**, *89*, 1208. (b) Ebelhauser, R.; Spiess, H. W. *Makromol. Chem.* **1987**, *188*, 2935.

(29) In some cases, including more component line shapes in the simulation does reduce the rough edges observed in some of the simulated spectra and produce a better fit. However, all the additional components have similar rates and gauche populations as one of the original components. Since our aim is to reveal the essential features of the dynamic processes rather than to achieve perfect fits, we have refrained from including additional components in our simulations.

(30) (a) Hirschinger, J.; Miura, H.; Gardner, K. H.; English, A. D. *Macromolecules* **1990**, *23*, 2153. (b) Miura, H.; Hirschinger, J.; English, A. D. *Macromolecules* **1990**, *23*, 2169.

(31) Kintanar, A.; Huang, W. C.; Schindele, D. C.; Wemmer, D. E.; Dorbny, G. *Biochemistry* **1989**, *28*, 282.

(32) Byrd, H.; Pike, J. K.; Talham, D. R. *Chem. Mater.* **1993**, *5*, 709.

(33) In accordance with our motional models, the "trans" and "gauche" states are mainly defined in terms of the orientation of the C_1-D bonds with respect to the three $P-O$ bonds in the headgroup, and the isomerization process involves rotational jumps around the $P-C_1$ bond. The observed fast rates could possibly arise from a much lower rotational barrier around $P-C$ bonds as compared to the barrier around $C-C$ bonds. Unfortunately, the lack of relevant rotational state data prevents us from comparing the magnitudes of the potential barriers.

(34) Textor, M.; Ruiz, L.; Hofer, R.; Rossi, A.; Feldman, K.; Hähner, G.; Spencer, N. D. *Langmuir* **2000**, *16*, 3257.

(35) Biswas, A.; Schürmann, B. L. *J. Chem. Phys.* **1991**, *95*, 5377.

(36) Biswas, A.; Schürmann, B. L. *Polym. Prepr. (Am. Chem. Soc., Div. Polym. Chem.)* **1992**, *33* (1), 562.